Damage induced by groundwater drawdown-related settlements on a Roman Aqueduct

M. Sangirardi[1], F. Rollo[2], G. Di Santo[3], Sara Barsoum[4] and A. Amorosi[5]

[1]Dr, University of Oxford, Department of Engineering Science. Oxford OX1 3PJ, UK. email: marialuigia.sangirardi@eng.ox.ac.uk
[2]Dr, Sapienza Università di Roma, Department of Structural and Geotechnical Engineering. Rome, Via Eudossiana 18, Italy. email: fabio.rollo@uniroma1.it
[3]MSc, Sapienza Università di Roma, Department of Structural and Geotechnical Engineering. Rome, Via Eudossiana 18, Italy. email: giacomo.disanto@uniroma1.it
[4]MSc, Sapienza Università di Roma, Department of Structural and Geotechnical Engineering. Rome, Via Eudossiana 18, Italy. email: barsoum.1848616@studenti.uniroma1.it
[5]Professor, Sapienza Università di Roma, Department of Structural and Geotechnical Engineering. Rome, Via Eudossiana 18, Italy. email: angelo.amorosi@uniroma1.it

ABSTRACT

Cultural World Heritage sites are increasingly at risk from climate change and the rapid infrastructure development driven by modern urbanisation, both of which heighten their vulnerability to surface settlements. While considerable attention has been devoted to the effects of tunnelling-induced settlements on surface structures in urban areas, comparatively less focus has been given to damage caused by ground subsidence.
In this study, we investigate the impact of surface settlements induced by groundwater extraction near an ancient Roman aqueduct. The hydraulic conditions are idealised, while the soil stratigraphy is inspired by the typical context of the Rome metropolitan area. The geometry and mechanical properties of the analysed structure reproduce those of the *Aqua Claudia*, a monumental 1st-century AD aqueduct, renowned for its advanced engineering and majestic arches.
The problem is addressed through coupled three-dimensional finite element analyses, in which the aqueduct is modelled accounting for its complex geometry and nonlinear structural behaviour. A recently developed multilaminate constitutive model is employed to capture the strength anisotropy associated with the inherent masonry texture.
The analyses aim to provide insights that extend beyond this specific case study. Considering the magnitude and distribution of the computed settlements, analogous implications can indeed be drawn for subsidence induced by different triggering mechanisms, including seasonal drying and shrinkage of soils or coastal movements induced by sea-level rise.

Keywords: Masonry, Damage, Groundwater Drawdown, Numerical Modelling, Settlements, Natural Hazard.

INTRODUCTION

Cultural World Heritage Sites represent an invaluable legacy of human civilisation, yet they are increasingly under threat from rapid urban infrastructure development and accelerating climate change impacts. In particular, surface settlements caused by deep excavations, tunnelling, and the modification of the hydraulic regime in soil deposits can cause significant damage to historical structures. Unlike modern infrastructures, which are typically built with reinforced materials and deep foundations designed to withstand significant ground movements, ancient masonry structures are highly brittle and sensitive to even minor differential deformations. Consequently, understanding and mitigating the structural risks associated with ground subsidence has become a key priority in heritage preservation.
An important trigger of extended ground subsidence is the extraction of groundwater. Aquifer pumping has become an unavoidable necessity, driven by the escalating demands of urbanisation and the exacerbating effects of climate change, which frequently disrupt traditional surface water supplies (Huning et al., 2024). From a hydrological and geotechnical perspective, the continuous withdrawal of water from subterranean aquifers disrupts the natural hydraulic condition of the soil deposit and modifies

the local hydraulic regime reducing pore-water pressures (e.g. Neuman & Witherspoon, 1969; Wen et al., 2008; Wang et al., 2026). According to standard consolidation theory, this results in an increase in effective stress and deformation of compressible layers, which ultimately manifests as regional or localised ground surface settlement (e.g. Su et al, 1998; Budhu & Adiyaman, 2010; Galloway & Burbey, 2011; Gambolati & Teatini, 2015).
While the understanding and prediction of the hydraulic mechanisms of subsidence is increasingly well-established, accurately translating these ground movements into structural damage through soil-structure interaction remains challenging. When an extraction-induced settlement trough reaches the foundation level, it drastically alters the contact stress distribution, imposing new kinematic constraints that force the structure to deform. Some studies showed the consequences of such differential settlements on modern structures, demonstrating how the relative stiffness of the soil-foundation-superstructure system dictates whether a building undergoes rigid-body tilting or severe shear-induced distortion (e.g. Díaz et al., 2018; Mayoral et al., 2019). However, evaluating these impacts on historical masonry structures reveals a critical gap in the literature. Furthermore, while considerable attention has been devoted to assessing the effects of tunnelling-induced settlements on surface structures in urban areas (e.g. Amorosi & Sangirardi, 2021; Pascariello et al., 2023; Zhao & DeJong, 2023), comparatively little focus has been directed toward the damage caused by broader groundwater subsidence. Although recent computational advancements have enabled accurate modelling of masonry vulnerability under general foundation settlement conditions (e.g., Gagliardo et al., 2021), coupled investigations that directly link the transient hydraulic regime of groundwater extraction to the nonlinear structural degradation of monumental heritage are lacking.
To address this gap, this study investigates the structural impact of surface settlements induced by groundwater extraction near a structure of high historical and archaeological significance. The idealised case-study features a simplified soil stratigraphy, inspired by the typical geotechnical context of the Rome metropolitan area. The presence of shallow formations characterised by soft clayey soils, and deeper layers of sand and gravel poses a relevant geotechnical problem related to the deformability of the fine-grained soils when water is extracted through wells installed in sand and gravel. The specific focus of the analysis is the evaluation of the damage that would be induced by water extraction on the ancient roman Aqua Claudia aqueduct. Its intricate geometry and specific material properties make this idealised - yet highly representative - case study a compelling example for understanding how monumental masonry infrastructure interacts with deep-seated ground deformations.
The problem is addressed herein through advanced, coupled three-dimensional finite element analyses to evaluate the distribution and the time evolution of settlements during the process of water extraction. A simple elasto-plastic constitutive model is employed to reproduce the compressibility of the thick, soft clay covering the coarse grained stratum where the water extraction takes place: hydro-mechanical analyses are performed to study the consolidation process occurring during and after the water extraction. Given the architectural intricacies of the Aqua Claudia aqueduct, the structure is modelled to rigorously account for its complex geometry and nonlinear structural behaviour under differential settlement. A crucial component of this numerical framework is the implementation of a recently developed multilaminate constitutive model for masonry to capture the strength anisotropy intrinsically associated with the inherent texture and block-and-mortar jointing of historical masonry. The effects of the ground settlements on the structural behaviour of the aqueduct are analysed, and a criterion of identification of the damage is proposed.

IDEALISED CASE STUDY

The structure analysed in this idealised case study is a well-known roman aqueduct. The construction of the *Aqua Claudia* began in 38 CE under Caligula and was then completed by Claudius in 52 CE. It represents one of the most technically ambitious portions of Rome's imperial water supply system. Extending for approximately 67 km from the upper Anio valley to Rome, it was designed to maintain a controlled gradient across complex topography, through a combination of underground and monumental elevated structures, among which, the most structurally significant section is the elevated approach to Rome. From the settling tanks (*piscinae limariae*) near Capannelle, the open channel (*specus*) was realised on continuous arcades, characterised by regular load distribution, pier spacing, and arch geometry, enabling both structural stability and material efficiency over long spans.
The aqueduct entered the city at *ad Spem Veterem* (Porta Maggiore), where the superimposed channels of the Aqua Claudia and Anio Novus illustrate the integration of multiple hydraulic lines within a single structural framework. The later incorporation of these arcades into the Aurelian Walls further attests to their robustness and long-term structural performance.

A section of the Aqueduct, adopted later as a modular unit to simplify the geometric reconstruction of the structure in this preliminary study, is reported in Figure 1a. Figure 1b shows some relevant dimensions, while Figure 1c reports the simplified discretisation used to assign the material properties to the structure. As it will be later discussed in more detail, the constitutive model adopted for masonry accounts for the internal structure of masonry and for the presence of preferential failure orientations which are located at the joints. For this reason, the arched portions are discretised in a finite number of homogeneous sections to which a common orientation of the failure planes is assigned. This is assumed to be parallel to the dotted lines reported in Figure1c for materials 2 to 7.

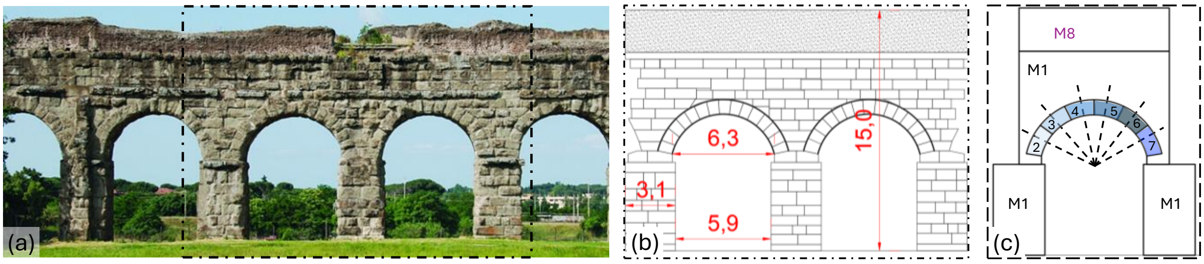

Figure 1. *(a) view of the Claudio Aqueduct, (b) relevant dimensions of the analysed structure (in m), (c) schematic representation of an arch-pillars module and materials definition.*

Figure 2 shows the stratigraphic sequence of the soil deposit on which the aqueduct rests. It is intended to represent a realistic yet idealised scenario, typical of recent alluvial basins found in the metropolitan area of Rome. Two main layers can be identified: a layer of silty clay at depths of up to 31 m, and a layer of sand and gravelly sand at depths of 31-45 m. Beneath this, there are very stiff Pliocene clays extending to significant depths. The ground water table is located at a depth of 5 m. The silty clay is characterised by a unit weight γ = 18.5 kN/m^3, a uniform void ratio *e* = 0.878, and hydraulic conductivity *k* = 10^{-7} m/s, while the sand is characterised by γ = 20 kN/m^3, *e* = 0.9, and *k* = 10^{-4} m/s. Both soils can be considered isotropic in terms of hydraulic conductivity. Figure 2 also shows the profile of the over-consolidation ratio (OCR) of the deposit.

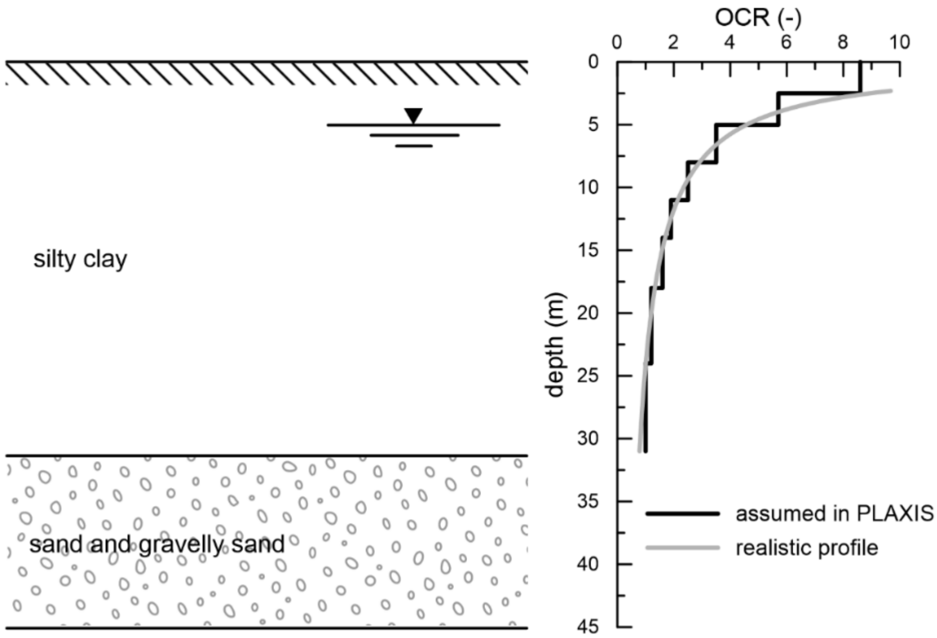

Figure 2. *(a) soil deposit and (b) profile of OCR with depth.*

The numerical model is built in the finite element code PLAXIS 3D (version 2024.3, Bentley, 2025). The plan dimensions of the soil volume are 1200m×1200m (Figure 3a), while the Aqueduct extends for 460m (Figure 3b). The thickness considered throughout the structure is equal to 2m. The model is discretised in 393621 10-noded quadratic tetrahedral elements, with 566249 nodes.

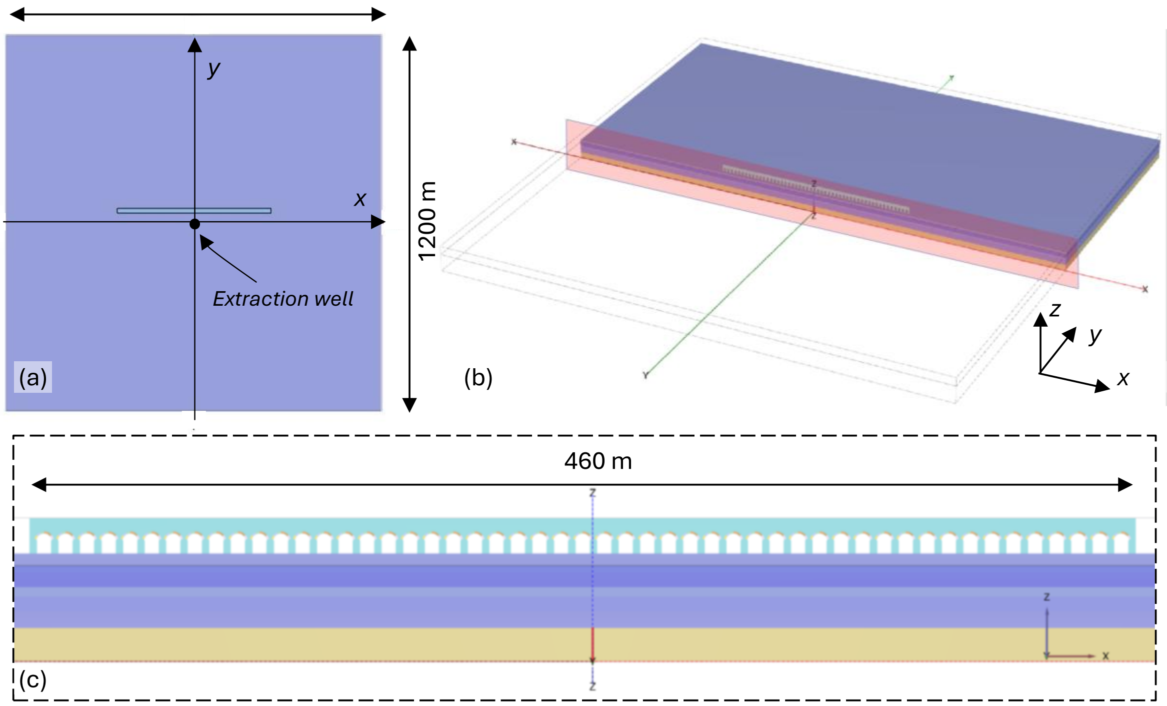

Figure 3. *(a) plan view of the numerical model, (b) analysed cross-section in a 3D view, (c) front view of the Aqueduct model.*

To account for the variation of OCR with depth, the layer of silty clay is divided in 8 sublayers to assign different uniform values according to the stepwise profile shown in Figure 2b. The structure is at a distance of 10 m from the well, which is located in the centre of the domain. The water extraction from the well is simulated through the *well* element available in the PLAXIS library. The outflow boundary condition is set to a constant value of 0.0048 m^3/s on the well element throughout the thickness of the sand layer to simulate the pumping of realistic flow rates. The hydraulic boundary conditions of the domain are set as open on the top and on the lateral surfaces, while the bottom surface is set as closed to simulate the impervious contour.

CONSTITUTIVE MODELS

The mechanical behaviour of the silty clay is reproduced by the single surface elasto-plastic *Soft Soil* model available in the library of PLAXIS 3D. The yield surface is the ellipse of the Modified Cam Clay model, combined with the Mohr-Coulomb failure criterion. The key features of the formulation are: (i) the isotropic hardening controlling the size of the ellipse via the volumetric plastic strain rates; (ii) a linear stress dependency of soil stiffness; and (iii) the distinction between primary loading and unloading-reloading. All the above make the model suitable for the description of the compressibility of fine-grained soils, while maintaining a few number of parameters and a simple formulation. The main internal variable, i.e. the preconsolidation pressure, is initialised according to the current stress state and the initial profile of OCR, while the parameters can be calibrated based on conventional laboratory tests, such as triaxial and direct shear tests for the soil strength, and on isotropic or oedometric compression to characterise soil compressibility. The sandy soil is modelled with a linear elastic perfectly plastic model with Mohr-Coulomb failure criterion. Table 1 shows the model parameters adopted in this study. The constants λ^* and κ^* are the compression and swelling indexes identifying the slope of the compressibility and swelling lines in the bi-logarithmic plane v-p', with v specific volume and p' mean effective pressure. The parameters c' and φ' denote the cohesion and the friction angle, ψ is the dilatancy angle, and E and ν are the elastic constants.

Table 1. *Constitutive properties adopted for the soils.*

Material	E (MPa)	v (-)	*c'* (kPa)	*φ'* (°)	*ψ*0 (°)	*λ** (-)	*κ** (-)
Silty clay (Soft Soil)	-	0.15	2	26	0	0.076	0.031
Sand (Mohr-Coulomb)	50	0.3	0.1	30	0	-	-

A recently formulated phenomenological elastic-perfectly plastic constitutive model, developed in the framework of simplified multilaminate anisotropic elasto-plasticity, is adopted for the masonry (Sangirardi et al., 2026). The model includes a phenomenologically sound mechanical interpretation of the plastic failure (tensile and shear failure) on the joints planes. The model is suitable for simulating the behaviour of regular-textured strong brick-weak mortar masonry, accounting for its anisotropic behaviour at yielding and for the interlocking effect leading to pseudo-tensile strength increase.
The elastic response is isotropic and linear, completely described by two elastic parameters determined through an analytical homogenisation procedure, as proposed in de Felice et al. (2010). The plastic anisotropic behaviour is introduced by means of a maximum of three planes on which the yield criterion can be attained according to a Mohr-Coulomb formulation with tensile cut-off.
The orientation of each plane in the 3D Cartesian space *xyz* is defined by the dip angle α_1 and the strike angle α_2 (Figure 4a). In this work, two planes (π_1 and π_2) are activated, oriented as the head and bed joints of a masonry wall (Figure 4b). The yield criterion of the generic *i*-plane is defined by three parameters: tensile strength $\sigma_{ti,0}$, cohesion $c_{i,0}$ and friction angle φ_{0i}. Dilatancy ψ_{0i} is set equal to zero for both plane 1 and 2.
The internal structure, accounted for by means of the width *b* and the height *a* of the blocks, is responsible for additional terms in the expression of the limiting shear and tensile strength on head joints (π_1) and bed joints planes (π_2), according to the following expressions in case of running bond texture, leading to the envelopes reported in Figure 4c and 4d for head joints and bed joints, respectively.
The strength domain on each plane is described by a Mohr-Coulomb criterion (f_{fi}) with a tension cut-off (f_{ti}), according to the following expressions, with i = 1,2:

$$\boldsymbol{f_{ti} = \sigma_{ni} - \sigma_{ti} \leq 0} \tag{1}$$

$$\boldsymbol{f_{fi} = \tau_i - c_i + \sigma_{ni}\, tan\, \varphi_i \leq 0} \tag{2}$$

where σ_{ni} is the normal stress component on the *i*-th plane, σ_{ti} is the tensile strength, ci is the cohesion, φ_i is the friction angle and τ_i is the resulting shear stress acting on the *i*-th plane, calculated from:

$$\boldsymbol{\tau_i = \sqrt{\tau_{ti}^2 + \tau_{si}^2}} \tag{3}$$

In this expression, τ_{ti} and τ_{si} are the two shear components on the plane considered, along the local axes *t* and *s*. At each step of the analysis, cartesian stress components are projected (according to the dip and strike angles earlier defined) on the pre-determined orientations.
Four failure mechanisms involving bed and head joints (all in plane) are considered for the identification of the updated values of σ_{ti} and c_i, calculated by imposing equilibrium conditions on the RVE. It is assumed that the friction angle is the same on both planes and does not change, thus $\varphi_i = \varphi_{i,0}$.
The whole derivation of the mathematical expressions of the strength parameters is here omitted for brevity and can be found in Sangirardi et al., 2026. The relevant equations are reported for tensile strength on head joints, and cohesion on bed and head joints, assuming that, due to bed joints geometry, as reported in Figure 1b, no interlocking affects the bed joints tensile strength, that remains equal to the initial value $\sigma_{t2} = \sigma_{t2,0}$.

$$\boldsymbol{\sigma_{t1} = \sigma_{t1,0} + \left(\frac{c_{2,0}}{tan\, \varphi_2} - \sigma_{n2}\right)\beta} \tag{4}$$

$$\boldsymbol{c_2 = c_{2,0} + \sigma_{t1,0}\frac{tan\, \varphi_2}{\beta}} \tag{5}$$

$$\boldsymbol{c_1 = c_{1,0} + \sigma_{t2,0}\frac{\beta}{tan\, \varphi_2}} \tag{6}$$

where $\boldsymbol{\beta = tan\, \varphi_2\,(b/2a)}$ is the coefficient accounting for the internal structure of the masonry that quantifies the interlocking effect. It should be treated as an additional constitutive parameter to be determined by visual inspection.
To comply with Mohr-Coulomb criterion constraints, the maximum tensile strength on head joints is calculated as:

$$\sigma_{t1,max} = \frac{c_1}{tan\,\varphi_1} \quad (7)$$

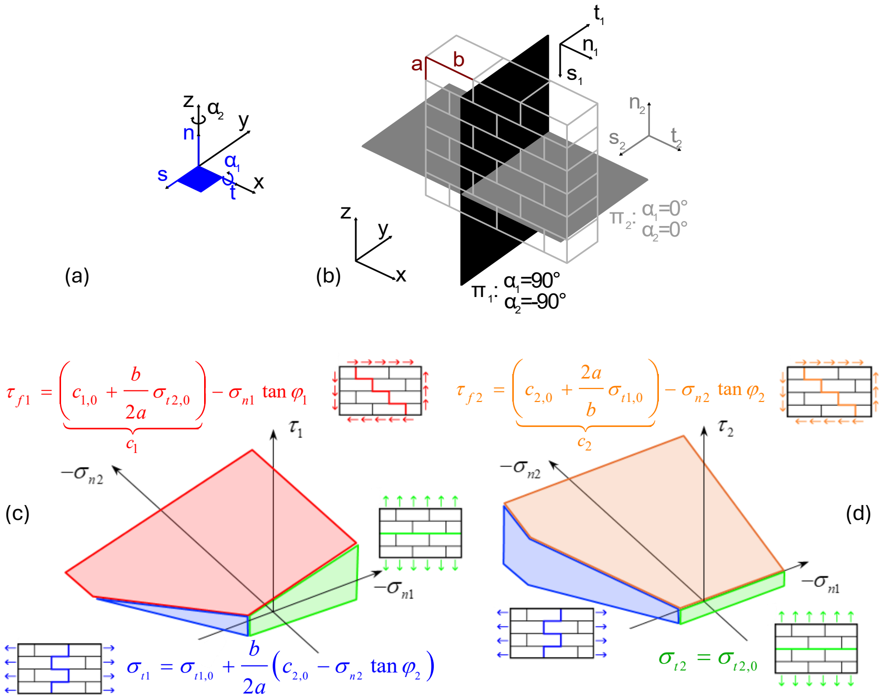

Figure 4. *a) Global reference, dip (α_1) and strike (α_2) angles, b) schematisation of the wall and planes orientation, strength domains on the c) head and d) bed joint planes and corresponding failure mechanisms.*

A linear elastic constitutive relation is assigned to the footing elements. The constitutive properties adopted for both the JMM-E and the linear elastic models are reported in Table 2.

Table 2. *Constitutive properties adopted for the structure.*

Material	**γ** (kN/m³)	**E** (MPa)	**ν** (-)	***β*** (-)	***c*₀ᵢ** (kPa)	***σ*₀ᵢ** (kPa)	***φ*₀ᵢ** (°)	***ψ*₀ᵢ** (°)
Masonry (JMM-E)	18	1200	0.1	1.08	50	25	30	0
Footings	18	1200	0.1	-	-	-	-	-

ANALYSIS PROCEDURE

The numerical procedure is structured in five different stages, briefly outlined below:

- *Stage 1*: activation of the soil deposit to initialise the internal variables of the models, and the geostatic stress state through the K_0-procedure;
- *Stage 2*: activation of the foundation elements of the aqueduct to reproduce in a simplified way the process of construction of the structure;
- *Stage 3*: construction of the superstructure of the aqueduct;
- *Stage 4*: steady-state flow analysis with a plastic calculation type to simulate water extraction at a constant flow rate in undrained conditions. The analysis aims at evaluating the excess pore water pressures generated in the silty clay as a consequence of the water extraction;
- *Stage 5*: consolidation analysis to achieve the complete dissipation of excess pore water pressure developed in the previous phase and to compute the evolution of the settlements at the foundation level of the aqueduct and the damage of the structure by means of plastic points location and maximum principal strains.

RESULTS: DAMAGE ON THE STRUCTURE

The resulting damage pattern after 10 days of consolidation (*Stage 5*) is reported in Figure 5 in terms of plastic points, together with the vertical settlements extracted at the level of the footings. It can be noted that the maximum vertical displacement is equal to around 25 cm, and that the differential settlement is equal to 15 cm. The settlements profile extends over a width of a few hundred meters.
Plastic points, representing Gauss points reaching the strength domain at specific locations (i.e. with specific yielding mechanism), mostly appear on the head joints in the columns (shear) and on the arches, here marking the occurrence of tensile failure. A few points highlighting damage associated to bed joints failure both in shear and tension, appear just above the most damaged arches and, as it will be shown in Figure 5, these are associated with high values of tensile strains (maximum principal), thus with more visible damage according to standard metrics (Boscardin and Cording, 1989).
Indeed, the observation of plastic points alone is not sufficient to fully describe the damage experienced by a structure, which should be quantitatively evaluated by means of strain proxies. However, neither strains alone would fully succeed in characterising the type of damage and the triggering mechanisms, which are conversely well described when plastic points are extracted.

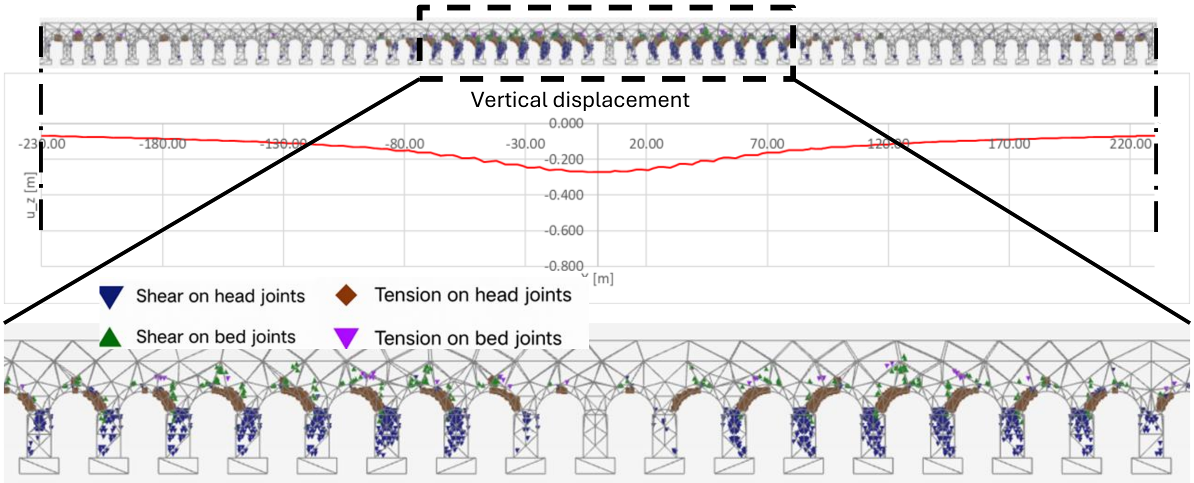

Figure 5. *Graph of the vertical displacements at the end of the consolidation phase (10 days) and plastic points pattern.*

A neater representation of the yielding mechanisms occurring in the Aqueduct is shown in the zoomed area of the structure, that is, between abscissas -75m and +75m. The "brown" plastic points (tensile failure on head joints, which are the only active plane for materials M2-M7) appearing at the arches are concentrating where hinges are expected to form and are a consequence of the relative displacement between adjacent pillars, as it can be easily observed in the vertical settlement profile.

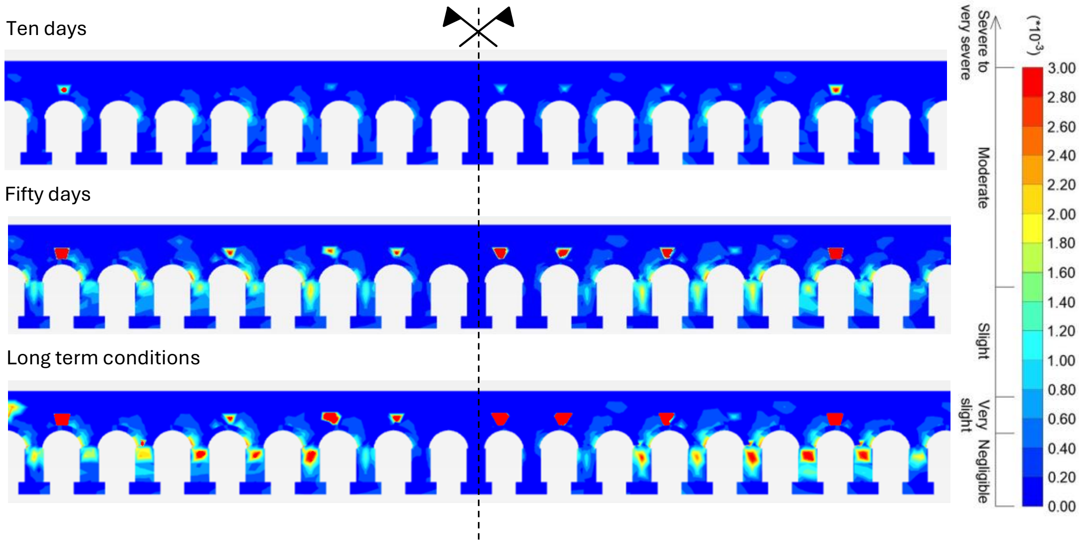

Figure 6. *Damage categories at different stages of the consolidation phase.*

The evolution of damage, represented in Figure 6 by means of maximum principal strains at different times (10 days, 50 days and long term), shows that first signs of slight damage already appear in the early stage (10 days) on the arches and above them, where the values of tensile strains indicate possible presence of visible cracks, especially towards the ends of the portion of the Aqueduct considered. In the intermediate (50 days) and long-term conditions, the damage remains slight on the arches but starts to involve the pillars and the central part of the structure, where cracks should be expected to appear.

CONCLUSIONS

It is recognised that settlements present a significant threat to existing masonry structures. Among possible anthropogenic sources of ground displacements, excavations and tunnelling are given a remarkable importance in the scientific literature. Less emphasis is devoted to possible effects of water extraction, which is indeed a widespread practice, often done with poor knowledge of possible consequences on the surrounding surface structures.

Because of their peculiar shape and extension, the settlements induced by water extraction are likely to induce negligible distortions and associated damage on “compact” structures. However, “long” structures, such as multi-span bridges or aqueducts, may be more vulnerable as this study demonstrates.

This paper presented an idealised case-study. As such, general conclusions should be drawn carefully, as many factors (both referred to the structure and to the soil stratigraphy) may alter the resulting scenario. In addition, the results presented herein specifically refer to pumping-induced settlements and to the investigated structural typology and loading conditions. Therefore, caution should be exercised when extending the findings to different subsidence-inducing mechanisms, such as seasonal shrinkage or coastal processes, whose temporal and spatial evolution, as well as settlement intensity, may substantially differ despite the common origin related to altered hydraulic conditions.

A coupled model accounting for both soil and structure nonlinearity was used to investigate the damage induced by the variation of hydraulic conditions in the subsoil following the extraction of water, highlighting that visible damage may appear on historic structures located in the vicinity of extraction wells. Remarkably, the process may last for a long time, with strains increasing progressively, leading to irreversible damage which should be appropriately predicted, quantified, and mitigated. Future developments will be addressed to a more systematic parametric study to examine the effect of water extraction on different structural typologies and different subsoil conditions.

REFERENCES

Amorosi, A., & Sangirardi, M. (2021). Coupled three-dimensional analysis of the progressive tunnelling-induced damage to masonry buildings: is it always worth it?. *Tunnelling and Underground Space Technology*, 118, 104173.

Bentley (2025). PLAXIS 3D 2024.3 General Information Manual.

Boscardin, M. D., & Cording, E. J. (1989). Building response to excavation-induced settlement. *Journal of Geotechnical engineering*, *115*(1), 1-21.

Budhu, M., & Adiyaman, I. B. (2010). Mechanics of land subsidence due to groundwater pumping. *International journal for numerical and analytical methods in geomechanics*, 34(14), 1459-1478.

de Felice, G., Amorosi, A., & Malena, M. (2010). Elasto-plastic analysis of block structures through a homogenization method. *International journal for numerical and analytical methods in geomechanics*, *34*(3), 221-247.

Díaz, E., Robles, P., & Tomás, R. (2018). Multitechnical approach for damage assessment and reinforcement of buildings located on subsiding areas: Study case of a 7-story RC building in Murcia (SE Spain). *Engineering Structures*, 173, 744-757.

Gagliardo, R., Portioli, F. P. A., Cascini, L., Landolfo, R., & Lourenço, P. B. (2021). A rigid block model with no-tension elastic contacts for displacement-based assessment of historic masonry structures subjected to settlements. *Engineering Structures*, 229, 111609.

Galloway, D. L., & Burbey, T. J. (2011). Regional land subsidence accompanying groundwater extraction. *Hydrogeology Journal*, 19(8), 1459-1486.

Gambolati, G., & Teatini, P. (2015). Geomechanics of subsurface water withdrawal and injection. *Water Resources Research*, 51(6), 3922-3955.

Huning, L. S., Love, C. A., Anjileli, H., Vahedifard, F., Zhao, Y., Chaffe, P. L., ... & AghaKouchak, A. (2024). Global land subsidence: Impact of climate extremes and human activities. Reviews of Geophysics, 62(4), e2023RG000817.

Mayoral, J. M., Tepalcapa, S., Roman-de La Sancha, A., El Mohtar, C. S., & Rivas, R. (2019). Ground subsidence and its implication on building seismic performance. Soil Dynamics and Earthquake Engineering, 126, 105766.

Neuman, S. P., & Witherspoon, P. A. (1969). Theory of flow in a confined two aquifer system. *Water Resources Research*, 5(4), 803-816.

Pascariello, M. N., Luciano, A., Bilotta, E., Acikgoz, S., & Mair, R. (2023). Numerical modelling of the response of two heritage masonry buildings to nearby tunnelling. *Tunnelling and Underground Space Technology*, 131, 104845.

Sangirardi, M., Di Santo, G., & Amorosi, A. (2026). An enriched and phenomenologically sound multilaminate model for masonry: JMM-E. *Engineering Structures*, *352*, 122113.

Su, M. B., Su, C. L., Chang, C. J., & Chen, Y. J. (1998). A numerical model of ground deformation induced by single well pumping. Computers and Geotechnics, 23(1-2), 39-60.

Tzampoglou, P., Ilia, I., Karalis, K., Tsangaratos, P., Zhao, X., & Chen, W. (2023). Selected worldwide cases of land subsidence due to groundwater withdrawal. *Water*, *15*(6), 1094.

Wang, C., Hu, J., Sun, J., Huang, F., Xiao, L., Wang, Q., & Bu, J. (2026). A Novel Semi-Analytical Model of Pumping Test With Depth-Decaying Hydraulic Conductivity. *International Journal for Numerical and Analytical Methods in Geomechanics*.

Wen, Z., Huang, G., Zhan, H., & Li, J. (2008). Two-region non-Darcian flow toward a well in a confined aquifer. *Advances in Water Resources*, *31*(5), 818-827.

Zhao, J., & DeJong, M. (2023). Three-dimensional probabilistic assessment of tunneling induced structural damage using Monte-Carlo method and hybrid finite element model. *Computers and Geotechnics*, 154, 105122.